# Infrared real-time-normalized photopyroelectric measurements of crystalline germanium: Instrumentation and spectroscopy

Constantinos Christofides, Andreas Mandelis, Kamyar Ghandi, and Robert E. Wagner
*Photoacoustic and Photothermal Sciences Laboratory, Department of Mechanical Engineering, and Ontario Laser and Lightwave Research Center, University of Toronto, Toronto, Ontario M5S1A4, Canada*

An infrared photopyroelectric spectrometer with real-time spectrum normalization capability measurements has been optimized and used for the spectroscopy of crystalline Ge, performed as a function of wavelength (1700–1960 nm) and modulation frequency (0.5 to 400 Hz), to determine the optical absorption and nonradiative quantum efficiency spectra. High-modulation-frequency (thermally thick limit: $f > 40$ Hz) data yielded the optical absorption-coefficient spectrum, while at low modulation frequency (thermally thin limit: $f < 15$ Hz) the nonradiative quantum efficiency spectrum was obtained self-consistently by substitution of the experimental optical absorption coefficient spectrum to the thermally thin limit photopyroelectric theory. The experimental results will be discussed in the light of an existing photopyroelectric model [A. Mandelis and M. M. Zver, J. Appl. Phys. **57**, 4421 (1985)] and in terms of well-established semiconductor germanium physics.

## I. INTRODUCTION

The phenomenon of pyroelectricity is not new, but was observed almost three centuries ago. The first measurements of the pyroelectric effect appeared shortly before World War I.[1,2] The use of pyroelectric detectors for the detection of infrared radiation was published by Yeou[3] in 1938. However, almost forty years passed before the first practical applications of a pyroelectric detector were reported.[4] In 1984 Coufal[5] and Mandelis[6] used for the first time thin pyroelectric polyvinylidene fluoride (PVDF) films for spectroscopic detection. Shortly afterwards, Coufal proved that photopyroelectric spectroscopy (P²ES) can be a very sensitive qualitative tool for thin film spectroscopic applications.[7] Tanaka[8] and Tanaka, Ichimara, and Sindoh[9] have shown that frequency-domain P²ES is also very promising for quantitative analysis.

Recently, P²ES has been used for the characterization of thin semiconducting films. Mandelis *et al.*[10] have performed spectroscopic measurements of an a-Si:H thin film on quartz. These authors further compared their experimental P²E spectra with similar spectra obtained by conventional, widely used photothermal deflection spectroscopy (PDS). This comparison showed the validity and nice performance of P²ES in addition to its unique capability for easy and self-consistent experimental acquisition of nonradiative quantum efficiency spectra.

As is well known, the optical absorption coefficient and the non-radiative quantum efficiency of semiconductors are of major interest because they provide information regarding the density and spectral activity of defect states in the material, particularly below the band-gap energy. Currently, there are two popular techniques employed for the determination of the optical absorption coefficient of semiconducting materials: transmission and photothermal deflection spectroscopies. However, transmission spectroscopy is limited to regions with a relatively large optical absorption coefficient; it is not easily applied in the sub-band-gap regions where the optical absorption coefficient is very small, and the difference between the incident and emergent signals is immeasurable. On the other hand, PDS allows for the measurement of even small optical absorption coefficients.[11] Thus a primary advantage of PDS over transmission spectroscopy is its higher dynamic range leading to the determination of much smaller absorption coefficients. However, PDS has limitations, such as the requirement for a coupling fluid, which may alter the surface characteristics of the sample under study or may exclude the spectroscopic applications of PDS to cryogenic temperatures. The consideration of these disadvantages, among others, led to the development of P²ES. As pointed out by several authors,[10,12] the main advantage of P²ES over other conventional photothermal spectroscopies is the fact that one can measure directly and self-consistently the optical absorption coefficient, $\beta(\lambda)$, and the nonradiative quantum efficiency, $\eta(\lambda)$, spectra.

This work establishes the above-mentioned dual spectroscopic capability of P²ES in the characterization of semiconducting substrates of finite thickness. It may be considered an extension of previously reported spectroscopy on thin semiconducting films.[10] The means of attaining this goal is the optimization of a dual channel P²E spectrometer and the quantitative investigation of crystalline Ge. Toward this end, P²E spectra have been recorded at various modulation frequencies. The experimental results will be discussed according to the photopyroelectric theory developed by Mandelis and Zver[13] and in terms of well-established semiconductor physics.

## II. THEORETICAL MODEL

In pyroelectric materials a change in temperature causes the release of electronic charges, thus changing the charge density and electrostatic potential on the surface. When the temperature change is due to the absorption, and subsequent thermal conversion, or optical radiation, the re-

sulting voltage across the material is the photopyroelectric effect. Pyroelectric materials are noncentrosymmetric solids (e.g., polyvinylidene fluoride and copolymers). Such materials may be fabricated into detector elements by poling in the presence of strong electric fields, so that the detector will acquire a net dipole moment relatively stable at room temperature, and by depositing thin metallic electrodes on the surface, which will carry away the extra charges by the (photo)pyroelectric effect when the element is operating as part of an electrical detection circuit.

The one-dimensional model developed by Mandelis and Zver[13] will be used for the interpretation of the output $P^2E$ signals presented in Sec. IV. Figure 1 presents the geometry of the photopyroelectric system. A solid sample (Ge in our case), of thickness $L_s$, is irradiated by monochromated light of wavelength $\lambda$, whose intensity is modulated at frequency $f$. If the pyroelectric film is optically opaque and thermally thick, and the surface reflectance is included in the form $A_s = 1 - R_s$, the photopyroelectrically detected voltage is given by the relation[13]

$$V(f,\beta_s) = \frac{pI_0 A_s}{2K\epsilon_0} \left[ \left( \frac{\beta_s \eta_s}{k_s(\beta_s^2 - \sigma_s^2)\sigma_p} \right) \{ 2(b_{sg}r_s + 1) - [(r_s + 1)(b_{sg} + 1) \exp(\sigma_s L_s) \right.$$

$$+ (r_s - 1)(b_{sg} - 1) \exp(-\sigma_s L_s)] \exp(-\beta_s L_s) \}$$

$$+ \frac{\eta_p \exp(-\beta_s L_s)}{k_p \beta_p \sigma_p} [(b_{sg} + 1)(b_{ps}r_p + 1) \exp(\sigma_s L_s) + (b_{sg} - 1)(b_{ps}r_p - 1) \exp(-\sigma_s L_s)] \left. \right] \Bigg/$$

$$[(b_{sg} + 1)(b_{ps} + 1) \exp(\sigma_s L_s) + (b_{sg} - 1)(b_{ps} - 1) \exp(-\sigma_s L_s)], \tag{1}$$

where $p$ and $K$ are the pyroelectric coefficient and the dielectric constant of the pyroelectric medium, respectively; $I_0$ is the light source irradiance incident at the solid surface; $\epsilon_0$ is the permittivity of vacuum ($8.85418 \times 10^{-12}$ C/V m); and $\eta_s$ and $\eta_p$ are the nonradiative conversion efficiencies (or heat conversion efficiencies) for the absorbing solid and the pyroelectric film, respectively. The index $j = g, s, p, b$ refers to the gas, sample, pyroelectric film, and backing, respectively. $\sigma_s = (1 + i)a_j$ with $i^2 = -1$, and

$$a_j = \sqrt{\pi f / \alpha_j} = \mu_j^{-1}, \tag{2}$$

where $\alpha_j$ is the thermal diffusivity and $\mu_j$ is the thermal diffusion length in material ($j$). The remaining coefficients are defined as[13]

$$b_{mn} \equiv k_m a_m / k_n a_n; \quad k_j: \text{thermal conductivity}, \tag{3a}$$
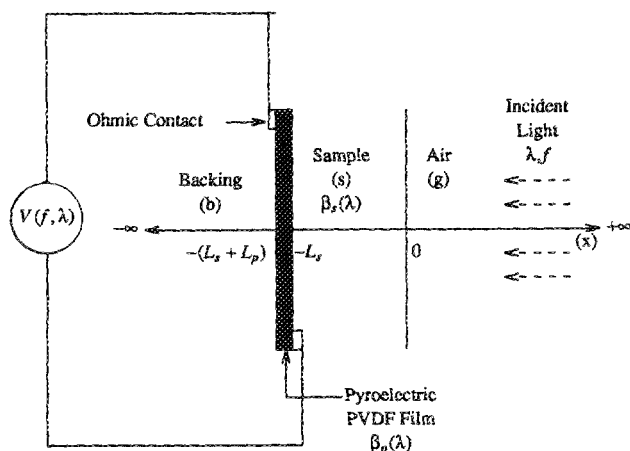
$$r_j \equiv \beta_j / \sigma_j. \tag{3b}$$

Finally, $L_s$, $\beta_s$ and $L_p$, $\beta_p$ are the thickness and the optical absorption coefficient of the sample and the pyroelectric film, respectively. In the absence of a sample, the $P^2E$ signal $V_R(f)$ generated by a thin-film blackbody nonreflecting reference directly deposited on the pyroelectric detector can be written in the form:

$$V_R(f) = \frac{pI_0}{2K\epsilon_0} \left( \frac{1}{k_p \sigma_p^2} \right) \tag{4}$$

upon setting $\eta_s = \eta_R = 1$, $A_s = 1$, $R_s = R_R = 0$, and $\sigma_s L_s \ll 1$, in Eq. (1).

The general Eq. (1) shows explicitly that the photopyroelectrically induced voltage, $V(f, \beta_s)$, is directly related to the optical and thermal parameters of the sample under investigation. However, due to the complexity of this equation, the mathematical deconvolution of the optical absorption coefficient and non-radiative quantum efficiency spectra is usually a difficult task. Therefore, we are going to distinguish two modulation frequency regimes in the case of a semiconducting sample of finite thickness, and for each case the optically opaque and transparent limits will be discussed.

## A. High modulation frequency—thermally thick limit: $L_s \gg \mu_s$

Setting $\exp(-\sigma_s L_s) \approx 0$ in Eq. (1) and dividing the result by the reference output signal [see Eq. (4)], the normalized signal ($V_N = V_s / V_R$) can be written as:

$$V_N(f, \beta_s) = A_s \frac{b_{ps}}{b_{ps} + 1} \left\{ \left[ 1 - \eta_s \left( \frac{r_s}{r_s - 1} \right) \right] \exp(-\beta_s L_s) \right.$$

$$+ 2\eta_s \left( \frac{r_s^2}{r_s^2 - 1} \right) \exp(-\sigma_s L_s) \left. \right\}. \tag{5}$$



FIG. 1. One-dimensional geometry of a photopyroelectric system.

### 1. Optically opaque sample: $\beta_s^{-1} \ll L_s$

In the optically opaque region $|r_s| \equiv \beta_s/\sqrt{2}\alpha_s \gg 1$. Upon setting in Eq. (5) $\exp(-\beta_s L_s) \approx 0$, the result gives the P²E saturation signal[13]

$$V_N(f) = 2\eta_s A_s \frac{b_{ps}}{b_{ps}+1} \exp(-\sigma_s L_s). \tag{6}$$

It follows that the amplitude and phase of the normalized P²E signal are

$$|V_N(f,\lambda)| = 2\eta_s(\lambda)A_s(\lambda)\left(\frac{b_{ps}}{b_{ps}+1}\right)\exp[-a_s(f)L_s], \tag{6a}$$

$$\Phi_D(f) = a_s(f)L_s = \sqrt{\pi/\alpha_s}\,L_s\sqrt{f}. \tag{6b}$$

We note that a plot of $\ln|V_N|$ vs $\sqrt{f}$ should yield a straight line with slope $= -\sqrt{\pi/\alpha_s}\,L_s$. Therefore, knowledge of the thickness of a sample leads to the measurement of the thermal diffusivity $\alpha_s$. Similar conclusions can be made with respect to the phase lag, Eq. (6b). $\Phi_D$ is the phase difference between sample and reference:

$$\Phi_D(f) = \Phi_s(f) - \Phi_R(f), \tag{6c}$$

where, in principle, $\Phi_R = \text{constant} = -\pi/2$. In experimental practice, however, $\Phi_R(f)$ includes all instrumental phase shifts in the P²E spectrometer and is used as a calibration curve.

### 2. Optically transparent sample: $\beta_s^{-1} > L_s$

For this case, we set in Eq. (5) $|r_s| \ll 1$. The result is

$$V_N(\beta_s) = |V_N(\beta_s)| = A_s(\lambda)\frac{b_{ps}}{b_{ps}+1}\exp(-\beta_s L_s). \tag{7}$$

Equation (7) presents a method for determining the optical absorption coefficient spectrum outside the P²E saturation region[13]

$$\beta_s(\lambda) = \frac{-1}{L_s}\ln\left(\frac{1+b_{sp}}{b_{sp}}\frac{1}{A_s(\lambda)}|V_N(\lambda)|\right). \tag{8}$$

### B. Low modulation frequency—thermally thin limit: $L_s \ll \mu_s$

Upon setting $\exp(\pm\sigma_s L_s) \approx 1$ in Eq. (1), division of the result by the reference expression given by Eq. (4) yields the normalized signal:

$$V_N(\beta_s,\eta_s) = A_s\left[\eta_s\left(\frac{r_s^2}{r_s^2-1}\right)[1-\exp(-\beta_s L_s)]\right.$$

$$\left. + b_{sp}\exp(-\beta_s L_s)\right]. \tag{9}$$

### 1. Optically opaque sample: $\beta_s^{-1} \ll L_s$

Setting $\exp(-\beta_s L_s) \approx 0$ in Eq. (9) and for large $r_j$ gives:

$$V_N(\beta_s,\eta_s) = V_N(\eta_s)_{\text{sat}} \approx \eta_s(\lambda)A_s(\lambda). \tag{10}$$

### 2. Photopyroelectrically nonsaturated sample: $\beta_s^{-1} > L_s$

In this case, $\exp(-\beta_s L_s) > 0$, and Eq. (9) may be written in polar coordinates:

$$V_N(\beta_s,\eta_s) = |V_N(\beta_s,\eta_s)|\exp[i\Phi_D(\beta_s,\eta_s)] \tag{11}$$

or

$$V_N(\beta_s,\eta_s) = A_s\left(\eta_s\frac{|r_s|^2\exp(-i\pi/2)}{|R|\exp(i\Phi_D)}\right.$$

$$\times[1-\exp(-\beta_s L_s)]$$

$$\left. + b_{sp}\exp(-\beta_s L_s)\right), \tag{12}$$

where $|R| = \sqrt{|r_s|^4+1}$, and $\Phi_D = \tan^{-1}(|r_s|^2)$. Equation (12) may be solved for the nonradiative quantum efficiency spectrum as a function of the real ($\text{Re}[V_N]$) and imaginary ($\text{Im}[V_N]$) parts of the normalized P²E signal:

$$\eta_s(\lambda) = \frac{\sqrt{\{\text{Re}[V_N(\lambda)] - b_{sp}\exp[-\beta_s(\lambda)L_s]\}^2 + \{\text{Im}[V_N(\lambda)]\}^2}}{A_s(\lambda)(|r_s|^2/|R|)\{1-\exp[-\beta_s(\lambda)L_s]\}}, \tag{13}$$

where values for $\beta_s(\lambda)$ may be substituted from the experimental spectrum obtained at the thermally thick limit (nonsaturated conditions).

## III. PHOTOPYROELECTRIC SPECTROMETER INSTRUMENTATION

Two experimental configurations were used to allow spectroscopic measurement in a wide range of modulation frequencies. In both cases, white light from a 1000-W Xe lamp was passed through a monochromator housing an infrared-blazed grating with a resolution of 16 nm which was adjusted using a stepping motor (step motor 2 in Fig. 2)

under IBM PS/2 computer control, to produce a beam with variable wavelength. The spectral cut-off filters associated with the monochromator were changed automatically using an electromechanical switch. Then the beam was focused and was directed towards the sample or reference detector. Using an oscillating mirror (M) the swept beam was alternately focused on two spots on a plane where the sample and detector would ultimately be placed. At those spots the beam sizes were approximately $1 \times 0.5$ mm² each in area. A special effort to minimize the size of the illuminated spot was made in order to maximize the irradiance of the incident radiation. The mirror was made to oscillate by a stepping motor (step motor 1 in Fig. 2) in the range of 0.1–15 Hz.
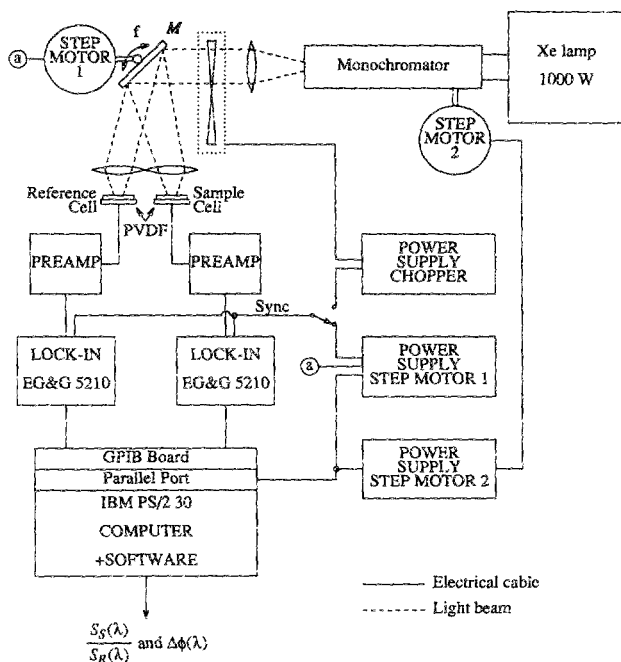
FIG. 2. Dual-channel photopyroelectric spectrometer instrumentation.

This modulation method is preferable to a beam splitter–mechanical chopper arrangement, since it avoids the wavelength dependence of the beam splitter. For frequencies in the range of 0.1–15 Hz the mirror oscillated automatically to provide modulation. However, for frequencies in the 15–600 Hz range, an EG&G chopper (Model 192) was placed before the mirror to provide the modulation while the mirror was controlled by the computer to switch from the sample to the reference detector, after a measurement at each wavelength was made. In this mode, the data acquisition software ensured that the intensity variation of the lamp during successive measurements of sample and reference did not contribute a considerable error. It is important to note that the two Al–Ni–PVDF photopyroelectric detectors were covered with black paint in order to absorb maximum optical flux (blackbodies). The two output signals were bandpass filtered and preamplified by two low-noise Ithaco preamplifiers (Model 1201). The two signals were then connected to a double-input Tektronix (Model T912) oscilloscope for visual display, and to two digital EG&G (Model 5210) lock-in analyzers (see Fig. 2). Depending on the configuration used, the reference for the lock-ins was obtained either from the oscillating mirror (0.1–15 Hz) or from the chopper (15–600 Hz). An IBM computer equipped with a mathematical coprocessor for fast calculations interacted with the two lock-ins through a GPIB board, and upon reading their output, it calculated amplitudes, and phases. Using only the two black PVDF films the normalized magnitude signal was further calibrated ($V_N \to 1$) at the beginning of each experiment by a judicious choice of gain on the preamplifiers, before placing the sample on one of the $P^2E$ detectors. Thus, before starting the experiments any detectable difference between the two photopyrolectric detectors was eliminated by the choice of the preamplifier gains.

The first reported experiments concerned spectrometer characterization. It was observed that the two PVDF detectors ("S": sample and "R": reference) sprayed with black paint, responded nearly ideally to the output light intensity of the Xe lamp: The two responses confirmed that the beams were indeed spectrally similar, and that any apparent differences in intensity could be corrected by the gain on the preamplifiers. These preliminary experiments have been performed at various frequencies in the range of 0.5–600 Hz in order to study the effect of modulation frequency on the differential $P^2E$ signal. It was shown that the spectrometer gives an excellent and reproducible response for frequencies lower than 400 Hz, while the signal-to-noise ratio (SNR) deteriorated at higher frequencies, due to the decreased light intensity and the introduction of acoustic noise generated by the EG&G mechanical chopper. It has been found that for frequencies lower than 400 Hz, the normalized signal $V_N$ from the two sprayed PVDF films is equal to one and the phase difference $\Phi_D$ is zero throughout.

For this study two different thicknesses of PVDF were used, 28 and 52 $\mu$m, in order to obtain thermally thick photopyroelectric conditions. The thickness of the PVDF and the experimental frequency must be such that the condition $a_p L_p \gg 1$ be satisfied, according to the definition of the thermally thick limit:

$$f \gg f_c \equiv a_p / \pi L_p^2, \tag{14}$$

where $f_c$ is the critical frequency, equal to 22 and 5 Hz, for PVDF thicknesses of 28 and 52 $\mu$m, respectively. Unfortunately, high thicknesses of PVDF such as 102 $\mu$m were impossible to use with the present housing configuration. As is well known,[14] the thermal time response of the PVDF film depends on its thickness, yet for our range of frequencies (0.5–400 Hz) this dependence is insignificant. The characterization experiments led to the conclusion that it is necessary to work in a frequency range greater than 5 Hz in order to satisfy the conditions of the theoretical model which is expressed by Eq. (1). For all subsequent experimental work 52-$\mu$m-thick PVDF was used in order to allow for the largest range of experimental frequencies, as well as to generate high output voltages.

In Eq. (4) one can write the output $P^2E$ voltage amplitude and phase from a blackbody thin surface film as

$$|V_R(f)| = \frac{pI_0}{2K\epsilon_0}\left(\frac{\alpha_p}{2\pi k_p f}\right), \tag{15a}$$

$$\Phi_R(f) = -\pi/2. \tag{15b}$$

Figures 3(a) and 3(b) present plots of the $P^2E$ amplitude and phase as a function of frequency. We note that the ln–ln plot of Fig. 3(a) plot yielded a straight line with a slope $-1$ in excellent agreement with Eq. (15a). On the other hand, the phase in Fig. 3(b) becomes almost constant for frequencies greater than 45 Hz, in agreement with the entirely thermally thick, constant behavior predicted by Eq. (15b). In order to account for the instrumental phase variation a certain calibration was required as a function of the working modulation frequency. However, one can avoid this problem by depositing a blackbody on the PVDF surface under a well-controlled evaporation method.
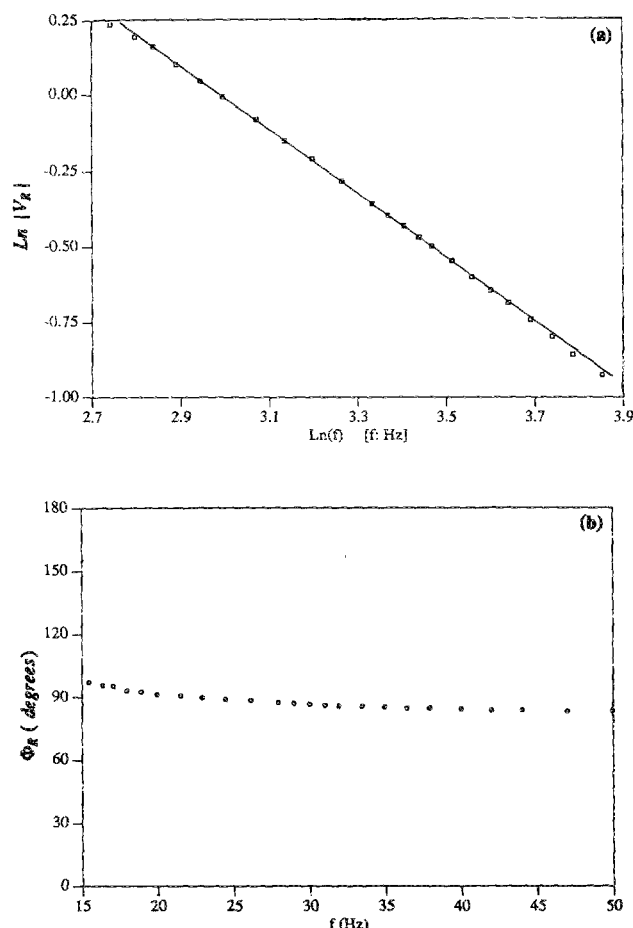
FIG. 4. Frequency dependence of the normalized $P^2E$ voltage amplitude $|V_N|$ as a function of the square root of the frequency for a $1250$-$\mu$m-thick Ge single crystal spray-painted black. Excitation source: white light from a $1000$-W Xe lamp.



FIG. 3. Frequency dependence of the reference (blackbody PVDF) $P^2E$ signal. (a) Logarithmic plot of the $P^2E$ normalized voltage amplitude as a function of the modulation frequency. (b) Frequency dependence of the reference phase difference $\Phi_R$.

## IV. PHOTOPYROELECTRIC SPECTROSCOPY OF GERMANIUM

For this study, Ge samples with crystalline orientation (111) were used. The samples themselves were squares of dimensions $4 \times 4$ mm$^2$. These samples were cut from a Ge ingot and wafers of thickness 1.25 mm were sawed and polished using a sequence of diamond pastes with slurry sizes down to 0.25 $\mu$m. The samples were put on the detector "$S$" and a gentle pressure was applied in order to have good PVDF-sample contact. Optical measurements have been performed across the band gap of Ge in the range of 1700–1960 nm. Unfortunately it was impossible to extend these measurements farther than 1960 nm because of limitations in the throughput of the Xe lamp.

### A. Frequency-dependent measurements

In the thermally thick limit it is obvious from Eqs. (6) that a good knowledge of the sample thickness $L_s$ yields a value for the thermal diffusivity:

$$\alpha_s = L_s^2 \pi \left( \frac{\Delta[\sqrt{f}]}{\Delta[\ln|V_N|]} \right)^2. \tag{16}$$

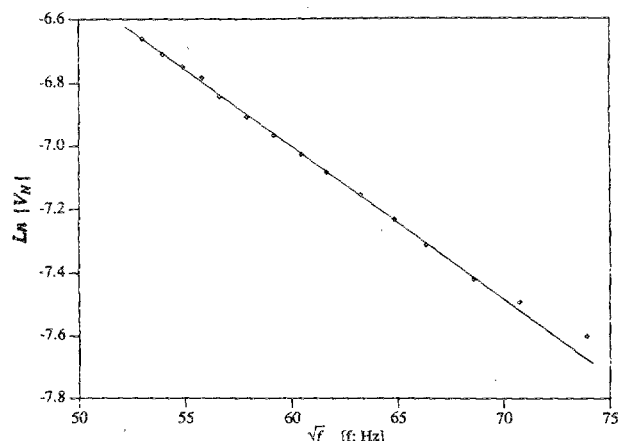A measurement of the slope of the straight line in Fig. (4)

and use of Eq. (16) yielded the value $\alpha_s \approx 0.22$ cm$^2$/s for the Ge thermal diffusivity, in relatively good agreement with published values.[15] It is important to note that this experiment was performed with white light excitation in order to increase the SNR. It was observed that even at very low wavelengths, such as $\lambda = 700$ nm, at which Ge is supposed to be strongly opaque there was a background signal that became progressively more important at high modulation frequencies where the thermal contribution is low. The origin of this signal is believed to be due to a residual piezoelectric behavior of the PVDF, which was under intimate mechanical coupling with the photopyroelectrically and photoacoustically excited sample. Thus, in order to avoid these kinds of problems at high modulation frequencies, the Ge sample surface was painted with a black paint in order to maximize the thermal wave contribution at loss of the direct transmission signal. The final experimental data taken as a function of frequency are presented in Fig. 4.

### B. P$^2$E infrared spectra

Figure 5(a) shows normalized $P^2E$ spectra of a Ge crystal obtained at 5, 14, 41, and 75 Hz at room temperature. The wavelength increment for data acquisition was one point every 5 nm. From the spectrometer sensitivity characterization point of view, it is important to note that these spectra have been obtained by the $P^2E$ spectrometer in a region were the throughput of the Xe lamp is very low (30–40 times lower than in the visible region). However, the experimental data were found to be very reproducible and the signal-to-noise level was satisfactory (40–200). As was expected from the transmissionlike nature of $P^2E$ signal near the bandgap at high frequencies,[13] the normalized $P^2E$ signal amplitude increased with increasing wavelength [see Fig. 5(a)]. In fact the signal in the transparent region was three orders of magnitude higher than in the opaque region. At low wavelengths the thermally thick normalized voltage is very small because in this case the signal depends mostly on the thermal contribution. On the other hand the thermally-thin $P^2E$ normalized voltage remains constant as a function of the wave-
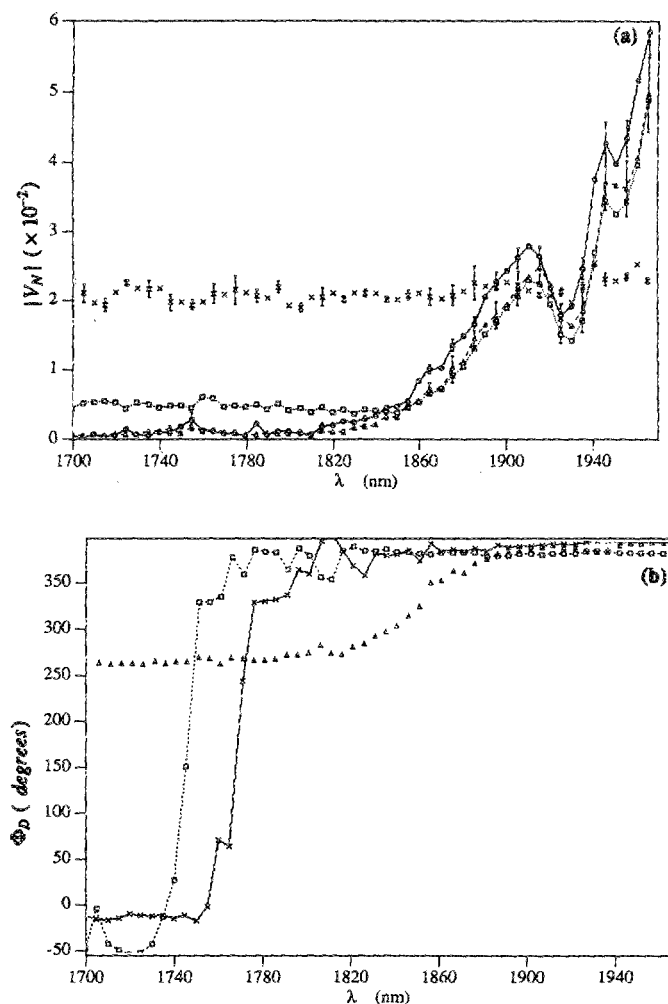
Photopyroelectric measurements

FIG. 5. (a) P²E normalized voltage $|V_N|$ spectra of Ge at various frequencies; $\times$: 5 Hz; $\cdots\square\cdots$: 14 Hz; $-\triangle-$: 41 Hz; and $-O-$: 75 Hz. Resolution 16 nm. (b) P²E differential phase spectra, $\Phi_D$, of Ge; $\triangle$: 14 Hz; $-\times-$ 41 Hz; and $-\square-$: 75 Hz. Resolution 16 nm.

for all frequencies, the phase difference $\Phi_D$ tends to the same values, due to the domination of the direct transmission signal over the photothermal absorption signal. (3) The absolute phase difference $\Phi_D$ is greater at higher frequencies, as expected from Eq. (6b).

## V. DISCUSSION

As stated earlier, one of the targets of this paper is to use the dual channel P²E spectrometer to determine the optical absorption coefficient and nonradiative quantum efficiency spectra of a crystalline Ge sample. In addition, in this section we will show that one can also evaluate the thermal diffusivity of the sample from the obtained P²E spectra with good precision. At high modulation frequencies (thermally thick regions) the normalized voltage is given by Eq. (7) which yields Eq. (8) for the calculation of the optical absorption spectrum $\beta_s(\lambda)$. In Fig. (6) we present optical absorption spectra of the Ge calculated from various curves of Fig. 5(a) and show that the long-wavelength spectra are reproducible at all frequencies. We note an excellent agreement between our experimental results and those obtained by other workers.[17-20] The absorption feature centered at 1933 $\mu$m does not appear in conventional transmission spectra of Ge.[17-20] It is believed to be a surface damage or contamination feature as a result of the fabrication and polishing process. This feature does not appear in the P²E phases of Fig. 5(b): such a correlation between amplitude and phase spectra would be expected from absorption features homogeneously distributed throughout the wafer bulk.[13] On the contrary, a surface feature may alter the amplitude of the photothermal signal, but its depth extent will not change the phase shift perceptibly if it is too thin.[21] $\beta_s(\lambda)$ exhibits photothermal saturation at high energies, the degree of which decreases with increasing modulation frequency, as expected.[13] In Fig. 6, $\beta_s$ decreases drastically around the region of the Ge gap at 1830 nm ($E = 0.66$ eV). Saturation takes place earlier at lower modulation frequencies than at high frequen-

length, thus indicating that a certain compensation between the thermal and direct optical transmission contributions takes place.

Figure 5(b) shows the phase difference $\Phi_D$ as a function of the wavelength, $\lambda$, for different frequencies (14, 41, and 75 Hz) at room temperature. These results have been obtained simultaneously with the data presented in Fig. 5(a). The following remarks can be made: (1) As was expected in the case of high modulation frequencies, when the band-gap region is approached $\Phi_D$ increases significantly as a function of wavelength, as the photothermal phase lag decreases due to the combined effects of the heat centroid moving closer to the back-surface detector[16] and the direct transmission signal becoming more significant. The latter effect is important at wavelengths where the sample is partially transparent, in other words, near the band gap. As the modulation frequency is increased, the wavelength at which the "transmission" signal becomes dominant shifts to lower values, since the absorption-related heat centroid signal is attenuated. This effect is experimentally illustrated in the above figure, as a phase jump occurring at shorter wavelengths when the modulation frequency is increased. (2) At high wavelengths and
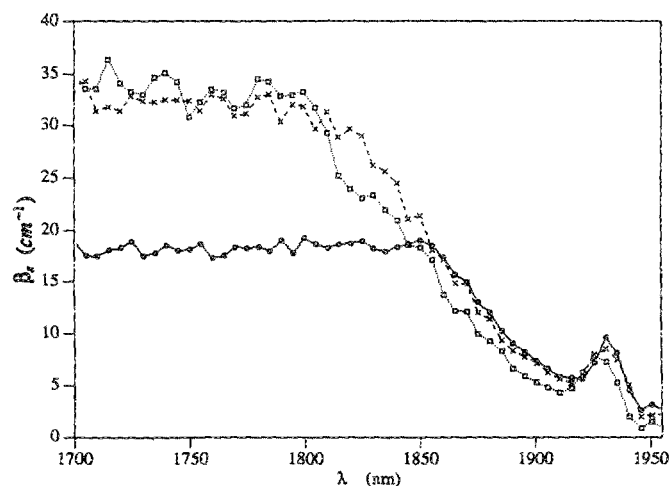


FIG. 6. Optical-absorption-coefficient $\beta_s(\lambda)$ calculation for Ge as a function of the wavelength. Data taken from curves of Fig. 5(a) at various frequencies: $-O-$: 14 Hz; and $-\times-$: 41 Hz; $\cdots\square\cdots$: 75 Hz.

Photopyroelectric measurements

cies (for example, at $\lambda = 1860$ nm when $f = 14$ Hz and at $\lambda = 1800$ nm when $f = 75$ Hz). In analogy to photoacoustic spectra,[22] in the limit of the saturated regime one can write

$$\frac{1}{\beta_c} \approx \sqrt{\frac{\alpha_s}{f\pi}}, \qquad (17a)$$

where $\beta_c$ is the critical absorption coefficient at the boundary between saturated and nonsaturated regimes. The value of the critical absorption coefficient $\beta_c$ increases when the modulation frequency increases in agreement with Eq. (17a). We note in Fig. 6 that $\beta_c$ is 18, 28, and 30 cm$^{-1}$ for spectra obtained at 14, 41, 75 Hz, respectively. In the following discussion we will take $\beta_c = 30$ cm$^{-1}$, which corresponds to $f = 75$ Hz and represents the saturation limit for all modulation frequencies up to 300 Hz. From Eq. (17a) the thermal diffusivity is given as:

$$\alpha_s = \pi f / \beta_c^2. \qquad (17b)$$

For $f = 75$ Hz, $\alpha_s \approx 0.26$ cm$^2$/s which is, within experimental error, consistent with the value found by the frequency-dependent measurements from Eq. (16) and Fig. 4. Similar results concerning the photoacoustic calculation of thermal diffusivity from optical absorption coefficient spectra have been published by McClelland and Kniseley.[23]

A discussion of the optical absorption coefficient profile of the 75 Hz curve will be given assuming a parabolic conduction-band density-of-states approximation for the band structure in Ge.

$\beta_s(hv)$ is then[19,20]:

$$\beta_s(hv) \propto (hv - E_g)^s/hv, \qquad (18)$$

where $s = \frac{1}{2}, \frac{3}{2}$, and 2 in the case of allowed direct transition, forbidden transition, and indirect transition respectively. $E_g$ is the energy of the optical gap. By taking $s = 2$ (indirect transition, which is the case with Ge in our working wavelength range), Fig. 7 shows a plot of $\sqrt{\beta_s hv}$ versus photon energy $E$. The drawn straight line is a least-squares fit to the data up to 0.68 eV and the intercept gives an energy gap of

0.652 eV. This value of $E_g$ is in agreement with the value previously reported in the literature ($E_g \approx 0.66$ eV).[17-20] The spectra range of the anomalous 1933 nm peak has been excluded from Fig. 7.

Finally, one can determine the nonradiative quantum efficiency spectrum from Eq. (13) upon substitution of the calculated $\beta_s(\lambda)$ in Fig. 6. In Fig. 8(a), we present the results obtained by using three different modulation frequencies: 14, 41 and 75 Hz. In the inset of Fig. 8(a) we present the log ($\eta_s$) vs $\lambda$ in order to show the variability of the nonradiative quantum efficiency (or heat conversion efficiency) even at wavelengths well above the bandgap. It is seen that $\eta_s$ increases substantially with a decrease in photon energy below the bandgap. Unfortunately, it is impossible to compare these experimental results directly with other data, since the 14 Hz (thermally thin) P$^2$E spectrum in this work gives the first such reported $\eta_s(\lambda)$ spectrum for Ge to the authors' best knowledge. However, two qualitative remarks can be made: (i) The spectrum of Fig. 8(a) anticorrelates with the quantum efficiency spectrum for Ge presented by Kirev[17]

FIG. 8. (a) Nonradiative quantum efficiency spectrum of crystalline Ge; from modulation frequencies ···□···: 14 Hz; and —○—: 41 Hz; -×-: 75-Hz P$^2$E spectrum. Inset: logarithmic spectrum. (b) Quantum efficiency spectrum of crystalline Ge (data taken from Ref. 17). $\Delta\lambda$: spectral range corresponding to part (a).
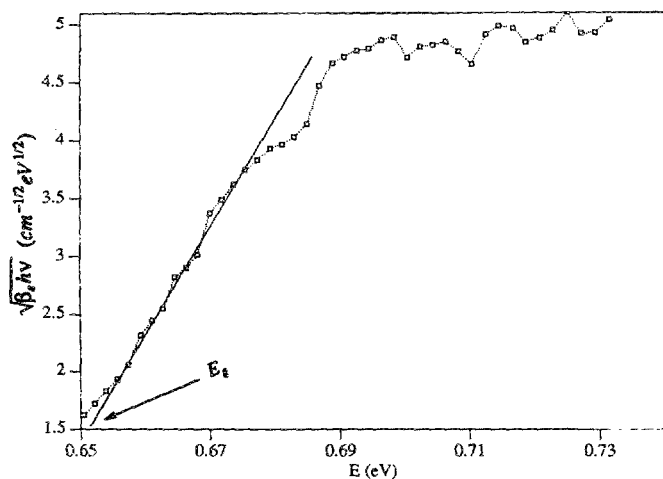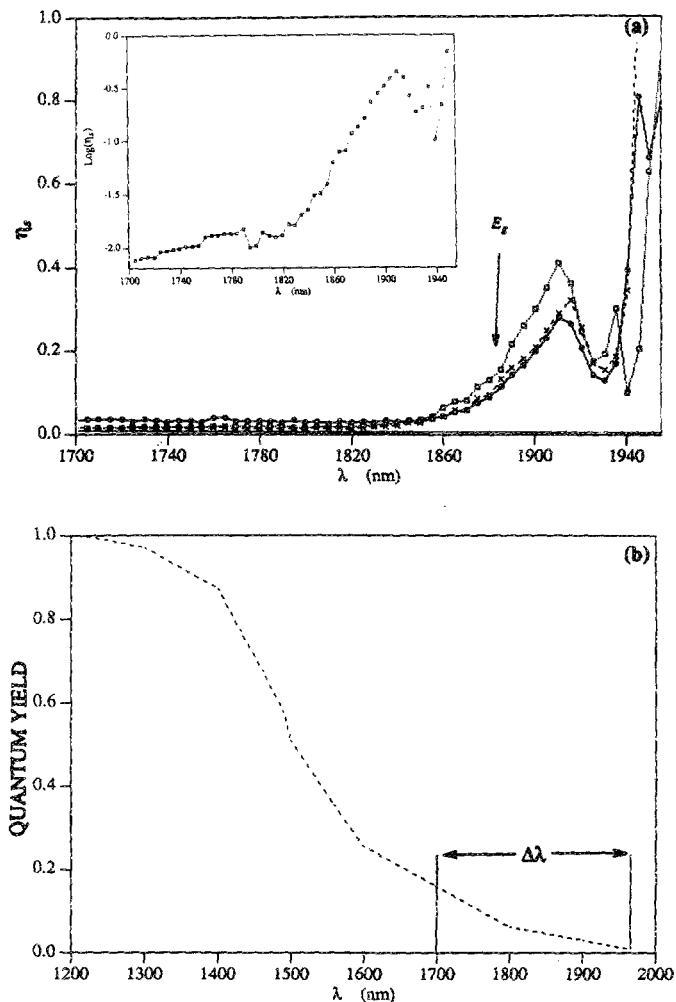
FIG. 7. Plot of the square root of the optical-absorption-coefficient, $\sqrt{\beta_s hv}$ as a function of the photon energy. Data taken from Fig. 6, spectrum at 75 Hz and does not include the anomalous peak region.

[see Fig. 8(b)], as would be expected from complementary electron deexcitation mechanisms (production of free carriers versus heat generation); (ii) Some results obtained photoacoustically by Kitamura, Ogawa, and Arai[24] using amorphous glass samples $(As_2Se_3)_{100-x}Ge_x$ led to spectral behavior of the nonradiative quantum efficiency across the optical gap qualitatively similar to our study: an increase of $\eta_s(\lambda)$ with increasing $\lambda$, below the optical gap of the glass. A more detailed physical analysis of $\eta_s(\lambda)$ spectra will be presented in a future publication. (iii) It is important to note that upon substitution of $\eta_s = 1$ (or some other constant) into Eq. (9), one finds that Eq. (9) cannot be solved for all values of $\lambda$, and even when the equation possesses a solution for $\beta_s$, the value was found to be different from the one obtained through Eq. (8) and presented in Fig. 6. This observation enforces the idea that the variation of the nonradiative quantum efficiency with wavelength must always be considered in photothermal spectroscopy in order to obtain self-consistent optical absorption spectra.

In this work, a new automatic, differential photopyroelectric infrared spectrometer has been characterized and used to evaluate the optical absorption coefficient and nonradiative quantum efficiency spectra of crystalline germanium. The two spectra have been obtained directly and self-consistently from $P^2E$ data at two different modulation frequencies satisfying the thermally thin and thick limit conditions, respectively. The ability of the theoretical model presented by Mandelis and Zver[13] to handle quantitative photopyroelectric spectroscopy of semiconducting samples with finite thickness has been demonstrated, consistently with its earlier success in analyzing thin-film spectra.[10] The main results of our study can be summarized as follows: (1) The dual-channel (real-time normalizing) photopyroelectric infrared spectrometer has been shown to be an excellent instrument for nondestructive evaluation of semiconductors of arbitrary thickness. (2) Simple, direct spectroscopic measurement of the optical absorption and nonradiative quantum yield spectra of Ge have been obtained. This ability and the absence of the solid-liquid interface, which may complicate, or interfere with, quantitative analysis[25] are important advantages over the well established PDS technique in semiconductor spectroscopy. It should be noted that these direct measurements can also be performed by other photothermal and photoacoustic spectroscopies, however, the price to be paid is considerable increase in the difficulty of the numerical analysis required to deconvolute the $\beta_s(\lambda)$ and $\eta_s(\lambda)$

spectra.[24] (3) The exploitation of the onset of $P^2E$ saturation in the optical absorption coefficient spectrum is a convenient method for the evaluation of the thermal diffusivity of the semiconducting sample.

## ACKNOWLEDGMENTS

[1]W. C. Roentgen, Ann. Phys. 45, 737 (1914).
[2]W. Ackerman, Ann. Phys. 46, 197 (1916).
[3]T. Yeou, C. R. Acad. Sci. 207, 1042 (1938).
[4]H. P. Beerman, Am. Ceram. Soc. Bull. 46, 737 (1967).
[5]H. Coufal, Appl. Phys. Lett. 44, 59 (1984).
[6]A. Mandelis, Chem. Phys. Lett. 108, 388 (1984).
[7]H. Coufal, Appl. Phys. Lett. 45, 516 (1984).
[8]K. Tanaka, in Photoacoustic and Thermal Wave Phenomena in Semiconductors, edited by A. Mandelis (North-Holland, New York, 1987), Chap. 16.
[9]K. Tanaka, Y. Ichimara, and K. Sindoh, J. Appl. Phys. 63, 1815 (1988).
[10]A. Mandelis, P. E. Wagner, K. Ghandi, R. Baltman, and P. Dao, Phys. Rev. B 39, 5204 (1989).
[11]D. Fournier and A. C. Boccara, in Photoacoustic and Thermal Wave Phenomena in Semiconductors, edited by A. Mandelis (North-Holland, New York), p. 237.
[12]H. Coufal and A. Mandelis, in Photoacoustic and Thermal Wave Phenomena in Semiconductors, edited by A. Mandelis (North-Holland, New York 1987), p. 149.
[13]A. Mandelis and M. M. Zver, J. Appl. Phys. 57, 4421 (1985).
[14]KYNAR Piezo Film Technical Manual, Pennwalt Corp., King of Prussia, PA (1983).
[15]Y. S. Touloukian, P. W. Powell, C. Y. Ho, and M. C. Nicolaou, in Thermophysical Properties of Matter (IFI/Plenum, New York, 1973), Vol. 10, p. 70.
[16]A. Mandelis, W. L. Lo, and R. Wagner, Appl. Phys. A 44, 123, (1987).
[17]P. Kirev, The Physics of the Semiconductors (Mir, Moscow, 1975), Chap. 8.
[18]S. M. Sze, Physics of Semiconductor Devices (Wiley-Interscience, New York, 1969), Chap. 2.
[19]J. I. Pankove, Optical Processes in Semiconductors (Dover, New York, 1971), Chap. 3.
[20]V. S. Vavilov, in Effect of Radiation on Semiconductors (State Press for Physical and Mathematical Literature Fizmalgiz, Moscow, 1963), p. 6.
[21]A. Mandelis, E. Siu, and S. Ho, Appl. Phys. A 33, 153 (1984).
[22]A. Rosencwaig, Photoacoustics and Photoacoustic Spectroscopy (Wiley-Interscience, New York, 1980).
[23]J. F. McClelland and R. N. Kniseley, Appl. Phys. Lett. 28, 469 (1976).
[24]M. Kitamura, T. Ogawa, and T. Arai, J. Phys. Soc. Jpn. 52, 2561 (1983).
[25]R. E. Wagner, V. K. T. Wong, and A. Mandelis, Analyst 111, 299 (1986).